

USGS 1-min Dst index

J.L. Gannon*, J.J. Love

USGS Geomagnetism Program, Denver, CO, USA

ARTICLE INFO

Article history:

Accepted 8 February 2010

Available online 15 February 2010

Keywords:

Magnetosphere
Ring current
Dst
Disturbance index

ABSTRACT

We produce a 1-min time resolution storm-time disturbance index, the USGS Dst, called $Dst^{8507-45M}$. This index is based on minute resolution horizontal magnetic field intensity from low-latitude observatories in Honolulu, Kakioka, San Juan and Hermanus, for the years 1985–2007. The method used to produce the index uses a combination of time- and frequency-domain techniques, which more clearly identifies and excises solar-quiet variation from the horizontal intensity time series of an individual station than the strictly time-domain method used in the Kyoto Dst index. The USGS 1-min Dst is compared against the Kyoto Dst, Kyoto Sym-H, and the USGS 1-h Dst ($Dst^{5807-45H}$). In a time series comparison, Sym-H is found to produce more extreme values during both sudden impulses and main phase maximum deviation, possibly due to the latitude of its contributing observatories. Both Kyoto indices are shown to have a peak in their distributions below zero, while the USGS indices have a peak near zero. The USGS 1-min Dst is shown to have the higher time resolution benefits of Sym-H, while using the more typical low-latitude observatories of Kyoto Dst.

Published by Elsevier Ltd.

1. Introduction

Ground-based magnetic field observations have a component that is reflective of the Earth's space environment and provide important information about the state of geomagnetic activity. The competing balance between Earth's intrinsic magnetic field and solar wind dynamic pressure drives much of the variation of the Earth's space environment (see, e.g. Russell, 2000). For example, sudden increases in solar wind density or velocity compress the day-side magnetopause, which result in enhancements and rearrangements of the complex current systems near the Earth. These current system changes are observed as magnetic field fluctuations at ground-level (McPherron, 1995).

The World Data Center in Kyoto uses ground-based magnetic field measurements to produce a global disturbance index called Dst, developed by Sugiura (1964). The Kyoto Dst index is used to characterize deviations from the quiet-time horizontal magnetic field during times of geomagnetic disturbance. It is produced with a 1-h time resolution and is continuous in time back to 1957. The index has been modified and improved over the years (e.g. Sugiura and Hendricks, 1967; Sugiura and Kamei, 1991; Karinen and Musula, 2006), but the essentially time-domain nature of the method has remained unchanged for over 50 years.

The Dst index is commonly used as an indicator of geomagnetic activity, including identification of storms, which have a critical influence on particle populations, satellites and other

human activity in space (e.g. Reeves et al., 2003). These storms have a classical multi-phase form observed in ground-based magnetic field measurements (Chapman, 1919), each having a distinctive shape and time scale: sudden commencement, initial phase, main phase and recovery phase. The sudden commencement occurs as the initial impact of increased solar wind dynamic pressure sharply compresses the magnetopause. At the ground, this is observed as a sharp increase in horizontal magnetic field intensity on time scales of less than 1 h. The main phase and recovery phases are characterized by a decrease in horizontal magnetic field intensity and then slow return to baseline. The strength of a geomagnetic storm is described by the minimum reached during the main phase (Gonzalez et al., 1994).

The 1-h time resolution of the Kyoto Dst is insufficient when researchers need to study effects that occur on sub-hour time scales, such as storm sudden commencements. The Kyoto Sym-H index is a 1-min time resolution index produced using a similar method as the Kyoto Dst (Iyemori, 1990). It provides higher time resolution than the Kyoto Dst, but Sym-H is inherently different because of the mid-latitude location of the observatories that are used. Because magnetic disturbance varies with latitude (Araki et al., 1997) and proximity to regional current systems contributes to the intensity of an observed magnetic signal, the Sym-H index can reflect different physical processes than a low-latitude index, especially during times of geomagnetic activity.

In this paper we apply the time and frequency space method of Love and Gannon (2009) to minute resolution horizontal magnetic deviation data from low-latitude magnetometer stations to produce a low-latitude Dst index with a 1-min time resolution. In the frequency domain, the observatory data display

* Corresponding author. Tel.: +1 303 273 8487.

E-mail address: jgannon@usgs.gov (J.L. Gannon).

a prominent set of stationary Fourier harmonics having periods equal to integer fractions of the Earth's rotational period, the Moon's orbital period, the Earth's orbital period, and the cross-coupling of harmonics with those periods. These harmonics dominate what is commonly described as solar-quiet variation, and are clearly identifiable in the frequency domain. Non-stationary contributions to the magnetic field time series, such as the secular variation of the Earth's magnetic field, are necessarily treated in the time domain. This index provides a measure of low-latitude disturbance with solar-quiet variation cleanly removed, and is produced with a sufficient resolution for analysis of physical processes with time scales less than an hour.

2. Data

Magnetic observatories are specially designed and carefully operated facilities that provide accurate data over long periods of time (e.g. Love, 2008). The data are collected using a digital acquisition system, and is combined with additional calibration data to produce time series that have long-term stability and accuracy, usually much better than 5 nT.

The Kyoto Dst index is calculated using hour resolution horizontal magnetic field intensity from four standard observatories chosen for their even longitudinal-spacing (Mendes et al., 2006), data quality, and continuity. Low-latitude (but not equatorial) positioning is also desired to avoid the signal from being dominated by the equatorial electrojet or auroral current systems. The observatories are Hermanus (HER) South Africa, Kakioka (KAK) Japan, Honolulu (HON) Hawaii, and San Juan (SJG) Puerto Rico.

In this analysis, we use the minute resolution horizontal magnetic intensity data to produce a 1-min resolution Dst index, calculated for the period 1985–2007. For simplicity and consistency with the Kyoto Dst, we use these same standard stations, although, in principle, we are not limited to these four. The 23 year reanalysis time span is chosen due to data availability of the minute resolution data, which extends back at least to 1985 for these observatories.

The percentage of missing data in each of the observatory time series is small (or literally zero for KAK). Operational changes resulting in abrupt offsets are usually well documented or easily identified upon inspection of the time series. The World Data Centers in Edinburgh and Kyoto and the Intermagnet consortium

provide definitive data which has been processed to remove baseline offsets and data spikes, at 1.0 and 0.1 nT precision, respectively. The time stamps are assigned at the top of the minute. Sym-H is obtained from the World Data Center in Kyoto, and uses data from varying combinations of mid-latitude stations.

3. Method

In this calculation we use the method detailed in Love and Gannon (2009), which combines time and frequency space analyses to isolate the disturbance signal from a magnetic field time series measured at a given observatory. Fig. 1 shows the data from the HON observatory, for the entire analysis time period of 1985–2007. There are multiple, overlapping magnetic field contributions that are reflected in the individual periodicities evident in the time series, as well as a long-term drift in intensity. The magnetic field horizontal component time series (H) is a superposition of contributions from the Earth's internal field and external current systems. The internal components mainly comprised slowly varying magnetic variations arising from the dynamo in the Earth's core (e.g. Jackson and Finlay, 2007) and also include contributions from the crust (e.g. Purucker and Whaler, 2007). For the purpose of this analysis, we label all long term, slowly varying drifts as secular variation (SV). The external components, including the non-periodic disturbance (Dist) signal, are composed of periodic contributions by ionospheric current systems (e.g. Campbell, 1989) and variations due to known periodic influences from the magnetosphere (SQ) and solar cycle (SC) (e.g. Clua de Gonzalez et al., 1993). In order to isolate Dist, we must first identify and remove the other contributing signals:

$$H = SV + Sq + SC + Dist. \quad (1)$$

The computational methodology outlined in Fig. 2 represents a summary of the process adapted to the minute time resolution data. We begin with the horizontal component magnetic field time series for an individual observatory. In each step, we remove one of the following components: secular (SV), solar cycle (SC) and solar-quiet (SQ) variation.

3.1. Internal contributions to magnetic signal—secular variation

We first identify and remove the most slowly varying components of the magnetic field time series—the secular

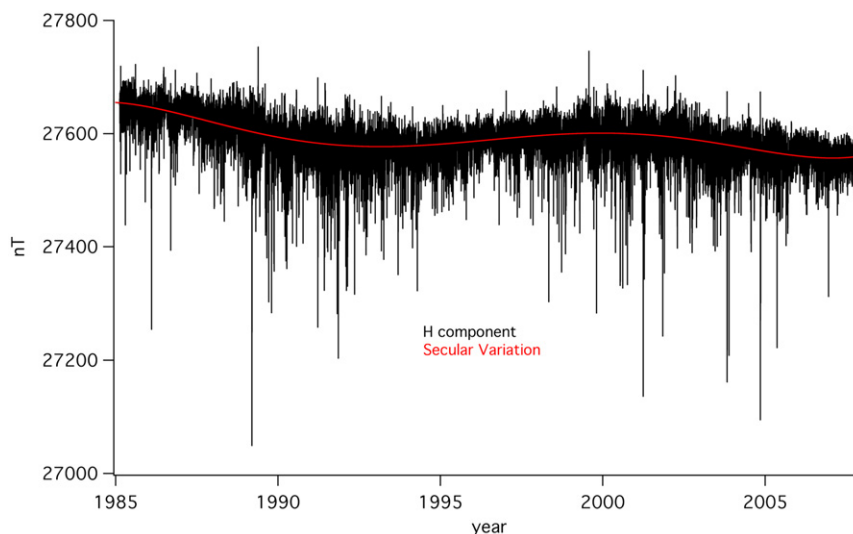


Fig. 1. Honolulu horizontal intensity (1985–2007). Overlaid is the estimated secular variation curve.

variation of the geomagnetic main field arising from convective fluid motion in the Earth’s core. This is seen in the observatory data as a slow drift in the magnetic vector over periods of decades.

Because no periodicities are resolved over the time span of this analysis, the identification of SV is done in the time domain. SV is not dependent on or affected by external current systems, and so

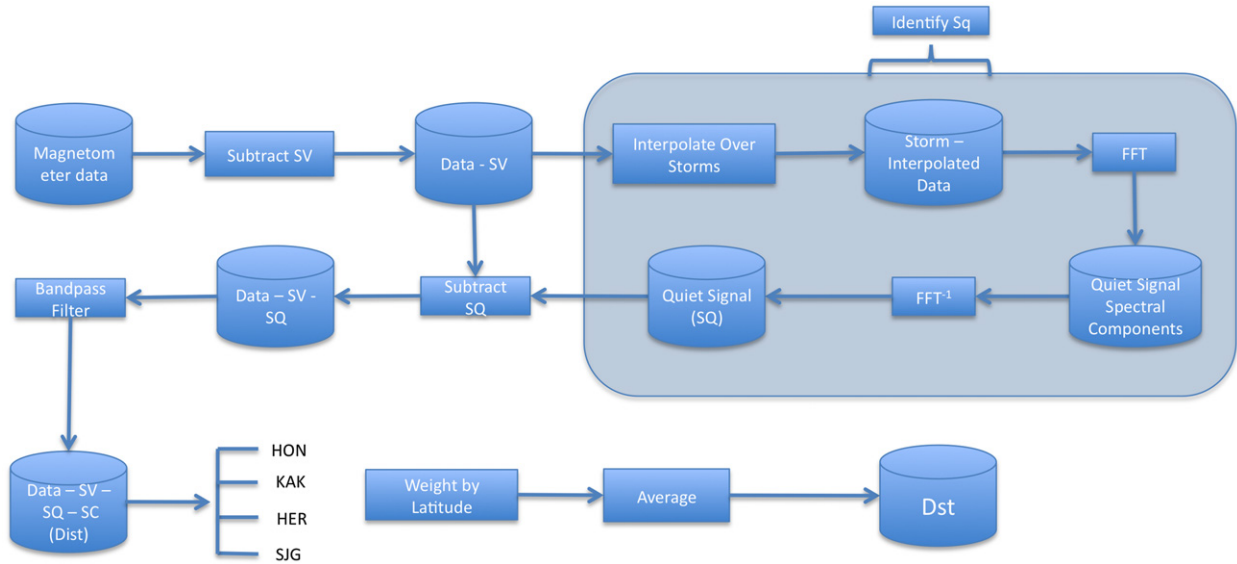


Fig. 2. Flowchart of USGS Dst calculation algorithm.

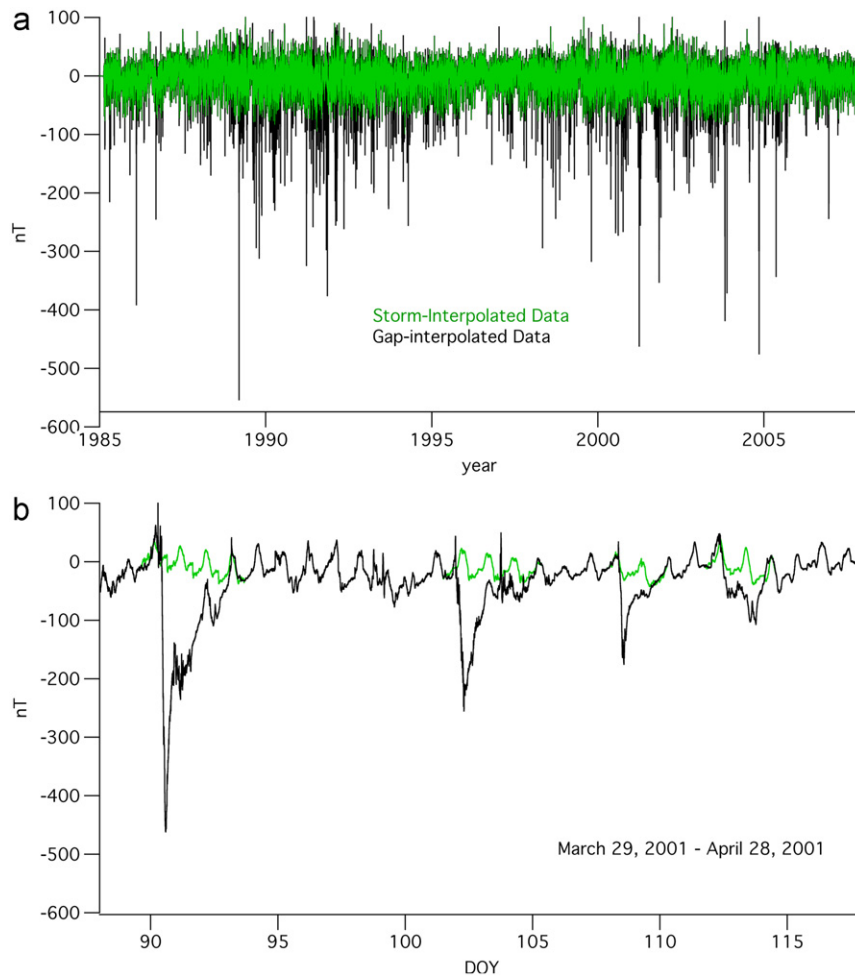


Fig. 3. Time series showing data with secular variation subtracted. Overlaid in green is the storm-interpolated time series. (a) shows the entire time span used in this analysis. (b) shows a close-up for the time period February 23–March 25, 2001, as an example. (For interpretation of the references to color in this figure legend, the reader is referred to the web version of this article.)

it is best identified during the quietest times of the time series, during which there should be the smallest contribution from external current systems. We use the following algorithm to select quiet days, using a 24-h sliding window, within which we measure the average of absolute hour-to-hour differences:

$$\delta H_i = \frac{1}{24} \sum_{m=1}^{24} \|H_{i+m} - H_{i+m-1}\|, \quad (2)$$

where the quantity is not calculated if more than half of the data are missing. For each month, the five smallest δH_i values determine the five quietest days, which we note do not necessarily correspond to whole universal-time days, nor do they necessarily correspond exactly to International Quiet Days, although there is often significant overlap. A truncated Chebyshev polynomial (Press et al., 2007) is fit to a time series of daily averages of the selected quiet-time periods and is subtracted from the observatory time series, effectively zero baseline detrending the data. In Fig. 1, the curve overlaying the observatory data shows the calculated SV polynomial for the HON time series. After the subtraction of SV, the time series contains only components due to external current systems and their inductive effects on the Earth (see Fig. 3).

$$H - SV = Sq + SC + Dist. \quad (3)$$

3.2. Solar-quiet variation

We identify solar-quiet variation as the periodic signals identified in the power spectrum seen in Fig. 4. These peaks in the spectrum are of relatively higher power than the surrounding frequencies, and can be identified as stationary Fourier harmonics having periods equal to integer fractions of the Earth's rotational period, the Moon's orbital period, the Earth's orbital period, and the cross-coupling of harmonics with those periods. We use a combination of time and frequency space techniques to isolate SQ and produce a time series which will be subtracted as the next step in the formulation of our Dst index.

We first do a rough cut of the disturbance signal in the time domain by selecting particularly disturbed time periods and interpolating across days during these times. This is done for each individual observatory time series by first ranking the hourly values of the $H - SV$ time series. Starting with the largest value, we open up a window of time that begins (ends) at least 12 h before (after)—the duration of the time window is at least 25 h in length, and its actual duration determined by a simple threshold criterion for maximum value within a sliding 12-h span of time. This enables us to define an active duration that commences before (ends after) the maximum point. We then remove all points from this identified active duration and substitute value interpolated between data corresponding to the same time-of-day according to

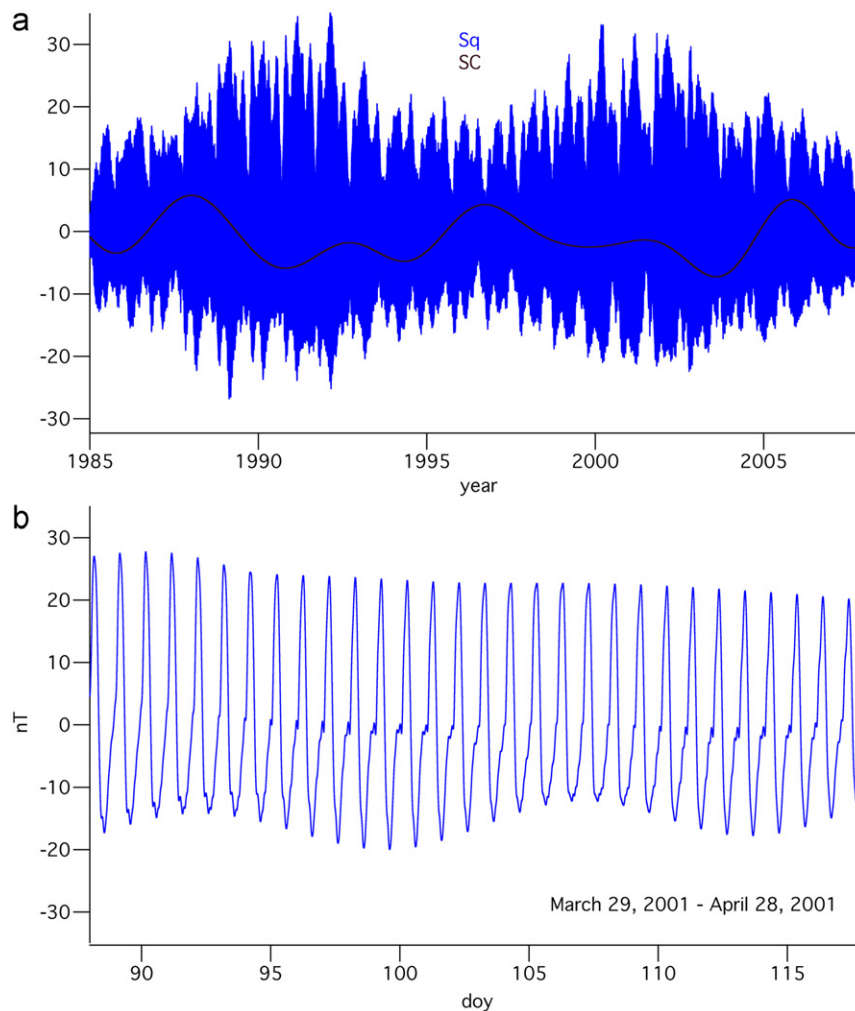


Fig. 4. Time series showing the solar-quiet variation, which is selected in the frequency domain. (a) shows the entire data span used in this analysis. (b) shows a close-up for the time period February 23–March 25, 2001, as an example.

the formula:

$$E_i = \frac{1}{m+n} (nE_{i-24m} + mE_{i+24n}), \quad (4)$$

where i denotes an instance in time, and m (n) is the number of days without missing data preceding (following) the day with missing data. The remaining values are then ranked again, and the process of disturbance identification and interpolation is repeated until a termination threshold is reached. Fig. 3(b) shows an example of this storm time interpolation. Note from Fig. 3(b) that both the storm-interpolated time series and the external signal have an obvious diurnal variation.

The storm-interpolated time series is then transformed to the frequency domain using a fast Fourier transform (FFT) (Press et al., 2007). The spectral peaks of components with periodicities that we consider to be solar-quiet variation are highlighted in Fig. 5(a). The peaks are well defined and are split due to modulation by other periodic influences. For example, the daily peak is evident at 1 day, and is flanked by a set of smaller peaks, due to spectral line broadening from modulation of the diurnal variation by solar cycle, the influence of the moon, and solar rotation. The Sq variation can be represented by a three-dimensional Fourier series of the form:

$$Sq(t) = \Re \left\{ \sum_{l,d,m,a} sq_{l,d,m,a} e^{i(l_d \omega_d + l_m \omega_m + l_a \omega_a)t} \right\}. \quad (5)$$

We band pass the Sq coefficients that correspond to narrow windows centered on each of these peaks in the frequency domain and reverse transform the selected components to the time domain using a reverse FFT to produce an SQ time series composed entirely of a signal of our selected frequencies, applying

the filtering to a finite number of harmonic terms. We adjust the width of the passing windows for each harmonic term so that, roughly speaking, the widest windows correspond to those frequencies having the greatest power.

We subtract the SQ time series (Fig. 4) from the external signal shown in Fig. 3 to yield a time series that contains the remaining SC and Dist signals.

$$H - SV - Sq = SC + Dist. \quad (6)$$

3.3. Solar cycle variation

We now identify, in the frequency domain, longer time period variations remaining in the time series from the solar cycle. This is a semi-periodic signal, but because of the variable length of the solar cycle, it will appear as a band of frequencies which are not well resolved using the data set available for minute resolution analysis. To remove long period variations, we transform again (this time using a time series where the highly disturbed periods are not removed) to frequency space and use a lowpass filter to remove all frequencies greater than 10 years. The components of SC are highlighted in Fig. 5 in the frequency domain.

The remaining components are transformed back to the time domain with all long period contributions removed (see Fig. 4). Although we do this in the frequency domain, it is equivalent to identifying SC frequencies, transforming the selection back to the time domain and subtracting it from the initial signal (Fig. 4 shows the SC curve in the time domain). This leaves us with the disturbance signal, Dist, for an individual observatory time series.

$$H - SV - Sq - SC = Dist. \quad (7)$$

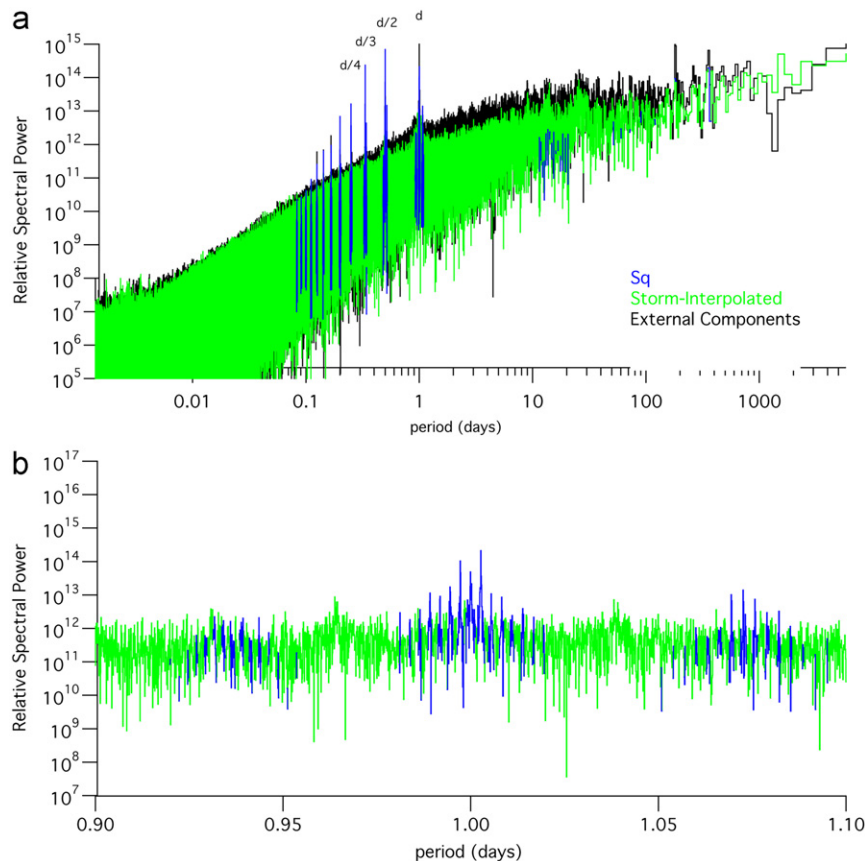


Fig. 5. Frequency-domain depiction of raw data and storm-interpolated data, with solar-quiet frequencies highlighted in blue. (a) shows the entire frequency space. (b) shows a close-up of the one day period. (For interpretation of the references to color in this figure legend, the reader is referred to the web version of this article.)

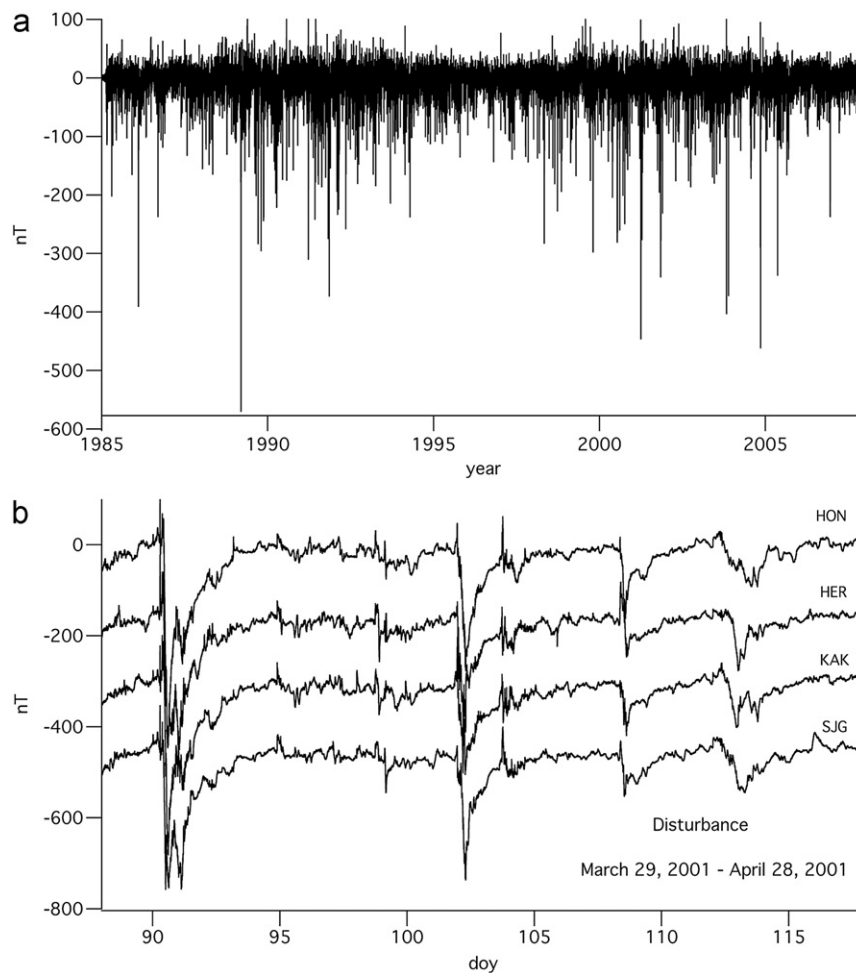


Fig. 6. Time series showing the data series with secular variation, solar-quiet variation and solar cycle variation subtracted. (a) shows the entire data span used in this analysis. (b) shows a close-up for the time period February 23–March 25, 2001, for the four standard observatories used in this analysis. Separation factors have been applied.

3.4. Disturbance signal

The remaining, isolated Dist signal is the deviation in horizontal magnetic field due to non-stationary changes in storm-time current systems. Fig. 6 shows the disturbance time series for HON, with Fig. 6(b) additionally showing the SJG, HER and KAK signals. Looking at Fig. 6(b), the diurnal signal that was obvious in Fig. 3 is now distinctly diminished. The differences between the Dist curves from different observatories are due to longitudinal variations in storm-time disturbance signal.

3.5. USGS 1-min Dst

The disturbance signals for individual observatories are now combined to produce our Dst index. Each time series station is weighted by $1/\cos\lambda_B$, where λ_B is the observatory site's magnetic latitude. The weighted time series are then averaged to produce the minute resolution Dst index, shown in Fig. 7. We will refer to this index, using this span of time (1985–2007) and this subset of stations (the four standard at the minute resolution, or 4SM), as $Dst^{8507-4SM}$. The time series in Fig. 7(a) and (b) look very similar to the individual magnetometer disturbance traces, with the four storms smoothly deviating from the quiet intervening periods, which contain no stationary periodic variation.

4. Analysis

4.1. Time series comparison

In order to understand the contributions of method and input to $Dst^{8507-4SM}$, we compare the time series to that of Sym-H, $Dst^{5807-4SH}$, and the Kyoto Dst (see Table 1 for a summary of the properties of each index). Sym-H has a 1-min time resolution like $Dst^{8507-4SM}$ and is used often when a higher resolution index is required for scientific analysis. It is produced by the World Data Center in Kyoto, Japan, following the essentially time-domain method of the hourly Kyoto Dst index, but using 1-min time resolution input from a set of mid-latitude observatories. Because of the known variation of geomagnetic disturbance propagation with magnetic latitude, we would expect the use of data from mid-latitude observatories to affect the final disturbance signal. Previous work by Wanliss and Showalter (2006) has shown that Kyoto Dst and Sym-H have reasonable correlation, diverging somewhat for values lower than -300 nT, and suggests that the benefits of the improved 1-min time resolution of Sym-H versus the 1-h Kyoto Dst outweighs any problems observed in Sym-H.

Fig. 10 shows an example time period, including the Halloween storm of 2003, for each combination of two indices. The overlaid green curve is the point-by-point difference between each pair of indices, where averaging is used when a time resolution difference exists. The main differences can be seen

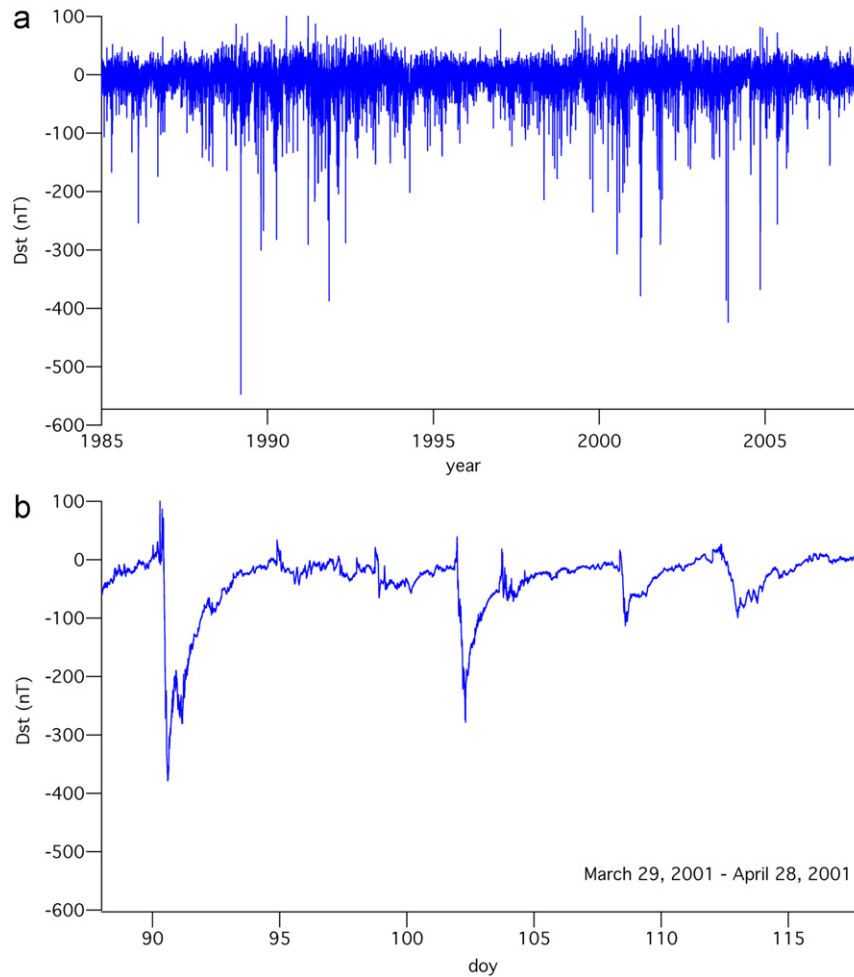


Fig. 7. Time series showing the calculated 1-min USGS Dst. (a) shows the entire data span used in this analysis. (b) shows a close-up for the time period February 23–March 25, 2001, as an example.

Table 1
Summary of index formulation.

Index	Method	Resolution	Input
$Dst^{8507-4SM}$	Time/frequency domain	1-min	Four standard low-latitude
$Dst^{5807-4SH}$	Time/frequency domain	1-h	Four standard low-latitude
Kyoto Dst	Time domain	1-h	Four standard low-latitude
Kyoto Sym-H	Time domain	1-min	Various mid-latitude

during storm main phase. The smallest storm-time differences appear between the two USGS indices. The largest storm-time differences occur between Sym-H and any other index. Sym-H also shows greater variability during the relatively quiet times surround the storm, when compared to the three other indices. To understand the general relative behavior of longer time series, we plot each index against each other. Fig. 11 shows correlation plots for the period 1985–2003 (the subset of time when the Kyoto Final Dst results are available), for pairs of indices. The overlaid line indicates perfect correlation, and in comparison we can quickly see how far each index deviates from the other with activity level. Sym-H and Kyoto Dst are highly correlated, and the two USGS indices (1-min and 1-h time resolution) are also highly correlated. In contrast, when comparing Sym-H and

$Dst^{8507-4SM}$, we see that Sym-H produces generally more extreme values than the USGS index during disturbed times. In the case of Sym-H versus $Dst^{8507-4SM}$, the hourly averaged indices are overlaid to facilitate a comparison to the other panels, where 60 times fewer points are available. There are some differences between Sym-H and $Dst^{8507-4SM}$ during times of higher activity that are particularly obvious using the un-averaged indices. The farthest outlying points correspond to the 2003 Halloween Storm. These deviations are less obvious on the hourly averaged comparison of the same two indices suggesting that the wide variation of Sym-H in comparison to hourly storm indices may have been previously understated, particularly during storm-time (Fig. 12).

Over the 23 reanalysis period, on average, Sym-H is 7.6 nT lower than $Dst^{4SH-8507}$. Fig. 13 shows the probability distributions of each index, further illustrating the differences. The shape of each distribution is similar, however indices of similar method (USGS 1-min/1-h and Kyoto Dst/Sym-H) have different peak distribution points. The USGS indices have a maximum likelihood of near 0, while for the Kyoto indices it is below zero.

4.2. Storm-time comparison

The previous sections described an overview of the available indices and a general comparison of the time series. In order to

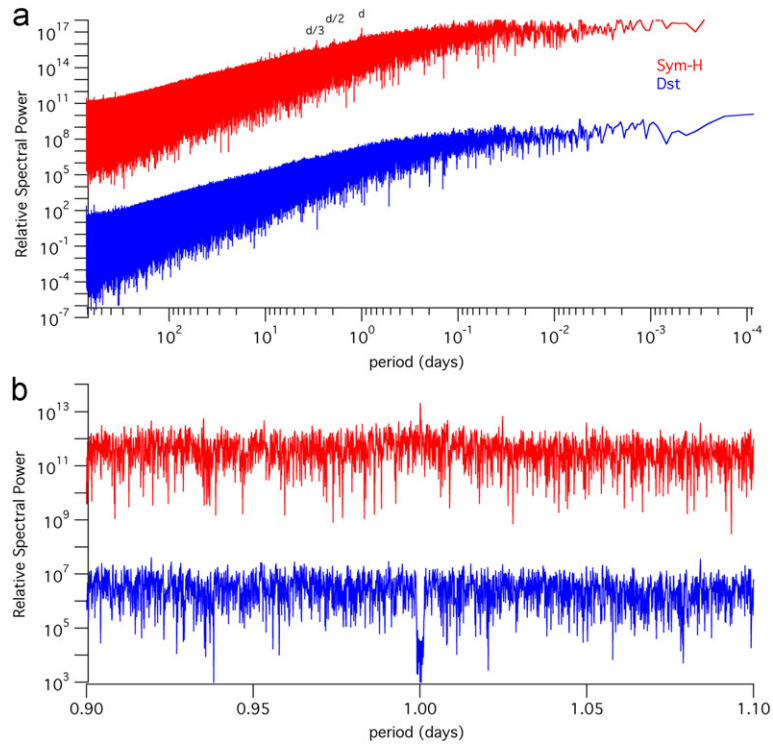


Fig. 8. Dst and Sym-H power spectra. (a) shows the entire frequency space. (b) shows a close-up centered on one day.

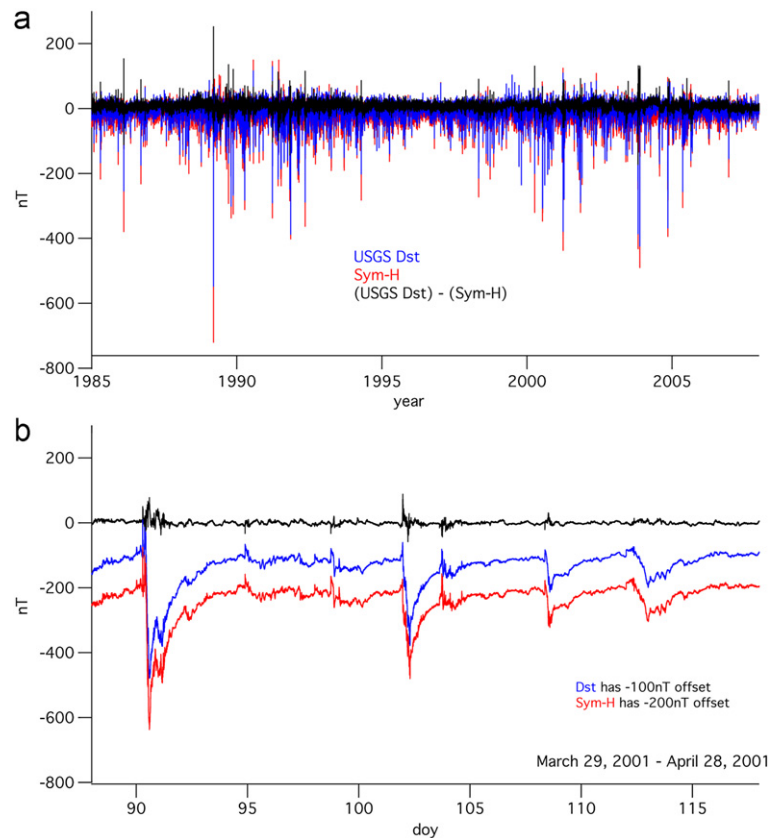


Fig. 9. Time series comparison of Dst and Sym-H. (a) shows the entire data span used in this analysis. (b) shows a close-up for the time period February 23–March 25, 2001, as an example. The black trace is the minute by minute difference between Sym-H and Dst.

look more closely at storm-time differences, we focus on the two 1-min time resolution indices, $Dst^{ASH-8507}$ and Kyoto's Sym-H. Fig. 9 shows a time series overlay of $Dst^{ASH-8507}$, Sym-H and the

minute by minute difference between the two. We can see from a close comparison in Fig. 9(b) that the largest differences occur during storm time sudden commencement and main phases.

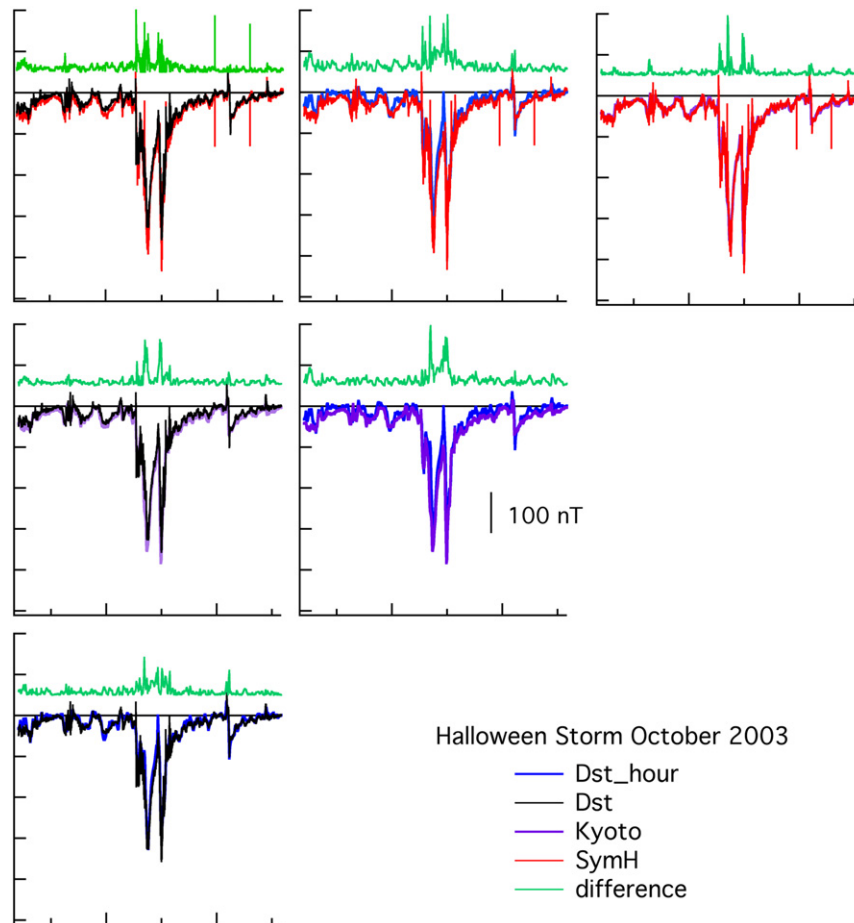


Fig. 10. Comparison of an example time series (including the Halloween 2003 storm) of each of the four following indices: USGS 1-min Dst, USGS 1-h Dst, Kyoto Sym-H, and Kyoto Dst against each other. The green curves in each panel are the difference between the two curves. For comparison of a 1-min index versus a 1-h index, 1-h averages are used. (For interpretation of the references to color in this figure legend, the reader is referred to the web version of this article.)

This difference suggests that, although the quiet-time baseline has been effectively (or at least similarly) removed, the disturbance signals contributing to the two indices can be greatly different in magnitude. This may be understood by considering the variation of different current systems with latitude. Based purely on contributions from an equatorial ring current, a lower magnitude would be expected for an index produced from mid-latitude stations (Mendes et al., 2006). However, our comparison shows that the contribution of mid-latitude effects to storm-time disturbance levels should not be underestimated.

The largest 10 storms for both indices are compiled in Table 2. Take as an example the March 1989 storm, which is ranked as largest by both the Sym-H and $Dst^{SM-8507}$ indices. During this storm, the main phase maximum deviation is -547.20 nT in the USGS 1-min Dst and -720 nT in Sym-H, a difference of nearly 200 nT. In general, Sym-H reflects a much larger maximum deviation during a typical storm main phase than our Dst.

4.3. Sudden impulse comparison

Sudden impulses are sharp peaks in the disturbance index time series which are responses to pressure increases in the solar wind. As a pressure pulse impacts the Earth, the dayside magnetic field is compressed. Particle populations in the ring current and radiation belts reconfigure and magnetopause currents are intensified in response to the inward pressure on the magnetopause. Changes in current systems result in a sudden enhancement

of the horizontal component of the magnetic field observed at the Earth's surface. These sharp increases often precede a magnetic storm, and are then termed sudden commencements. Using an hour resolution index during these times these important features are unresolved. Fig. 13 b shows a comparison of the 1-min Sym-H and $Dst^{8507-4SM}$ versus the 1-h $Dst^{5807-4SH}$ and Kyoto Dst for the large sudden commencement preceding the large storm at the end of March 2001. Both hourly indices completely miss the sudden commencement, which is greater than 100 nT in both the minute resolution indices. Fig. 13 c shows a close-up of the minimum of the same storm.

Analyses requiring higher resolution information sometimes use minute resolution horizontal-component magnetometer traces (e.g. Araki et al., 1997). In some cases, using individual traces provides additional spatial information about impulse propagation. When a global picture of storm-time magnetic field development is desired, an index such as Sym-H can be used. However, as previously mentioned, the mid-latitude positioning of the stations used in the formulation of Sym-H can have an impact on the final result, particularly during times of high geomagnetic activity (see Table 3). Comparing the magnitude of the Sym-H index during active times to that of $Dst^{8507-4SM}$, we find that, as in the storm main phase intensities comparison, Sym-H reflects a more extreme deviation than $Dst^{8507-4SM}$. For example, in July of 1990, the maximum SI value of Sym-H is 149 nT, while $Dst^{8507-4SM}$ reaches only 115.5 nT. The difference between the two indices also seems unrelated to the size of the event. Sym-H also reached 149 nT in June of 1991, when $Dst^{8507-4SM}$ was only

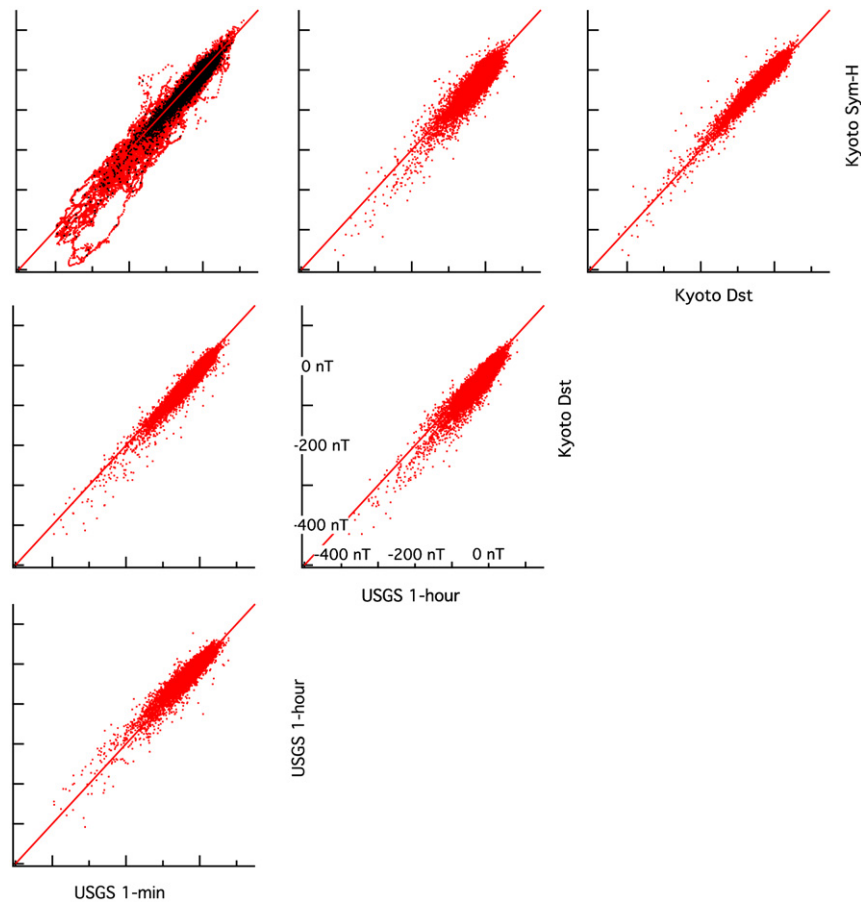


Fig. 11. Correlation plots for pairs of the four indices (USGS 1-min Dst, USGS 1-h Dst, Kyoto Sym-H, and Kyoto Dst), for the period 1985–2007. For comparison of a 1-min index versus a 1-h index, 1-h averages are used. In the top left panel, USGS 1-min vs Kyoto Sym-H, the comparison of the 1-h averages is overlaid in black to facilitate comparison with the other panels.

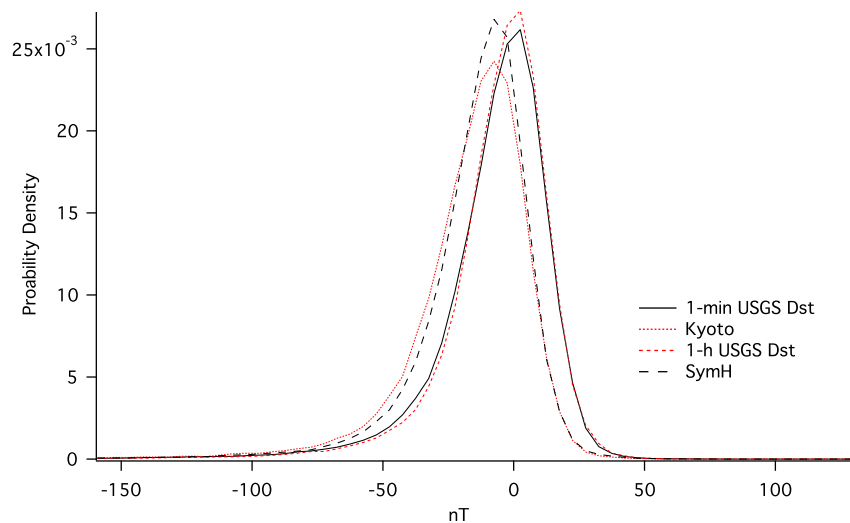


Fig. 12. The probability distributions for each of the four indices (USGS 1-min Dst, USGS 1-h Dst, Kyoto Sym-H, and Kyoto Dst).

86.6 nT. In other words, the two indices are not linearly related to each other. A large SI in Sym-H may correspond to a large SI in Dst, or it may not. We also see that the hourly indices of USGS and Kyoto are well correlated during these times (see example, Fig. 13), suggesting that the difference between Sym-H and $Dst^{8507-4SM}$ lies not in method, but in the latitudinal differences of the observatories contributing to the product.

4.4. Spectrum comparison

In addition to time series comparisons of $Dst^{4SH-8507}$ and the Kyoto Dst, we can use the same frequency-domain techniques we exploited to precisely identify and excise Sq to compare the spectral components of each index and look for remaining spectral peaks in either index. In Fig. 8(a) the power spectra of

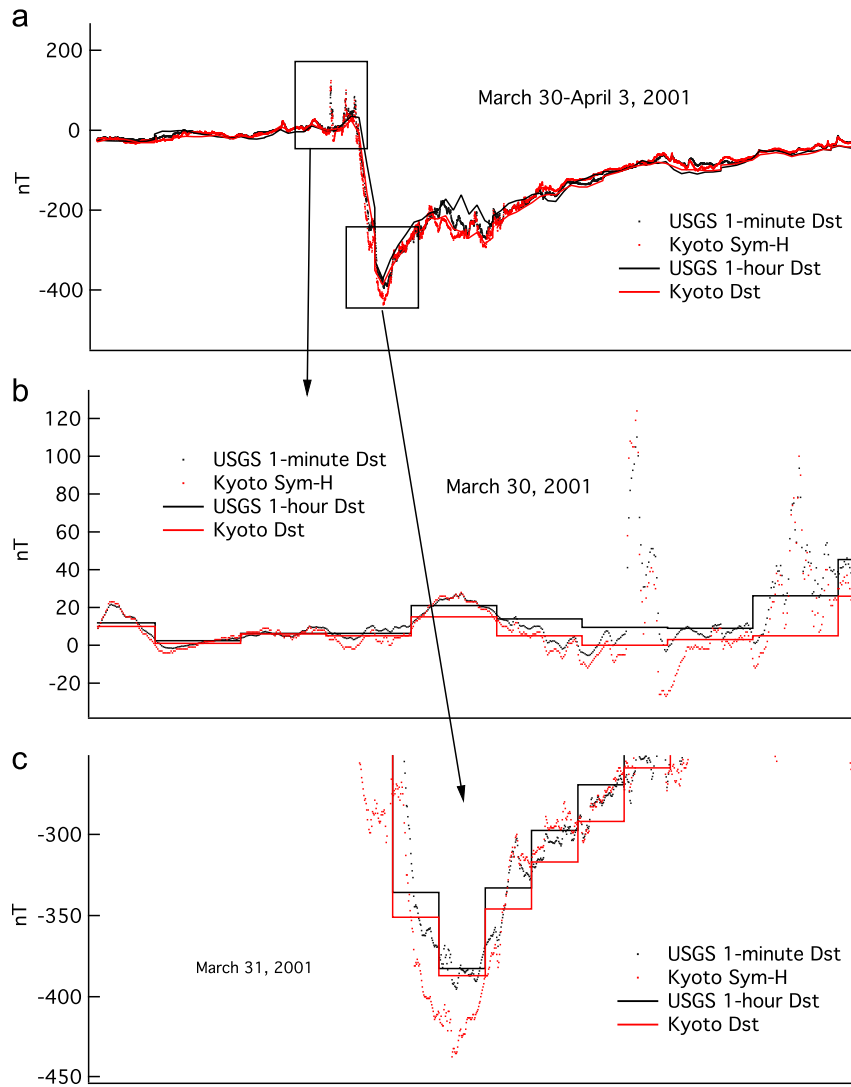


Fig. 13. (a) Comparison of how well the four indices (USGS 1-min Dst, USGS 1-h Dst, Kyoto Sym-H, and Kyoto Dst) resolve short time scale fluctuation. (b) is the large sudden commencement preceding a large storm at the end of March 2001. (c) is the minimum of the same storm.

Table 2
The 10 largest main phase deviations for the Dst index and the corresponding value of Sym-H, 1985–2007.

yyyy/mm/dd	Dst (nT)	Sym-H (nT)
1989/3/14	-547.2	-720
2003/11/19	-423.6	-490
1991/11/8	-387.0	-402
2003/10/28	-385.7	-432
2001/3/29	-378.3	-427
2004/11/3	-367.3	-394
2000/7/11	-306.5	-347
1989/10/20	-300.4	-337
1991/3/23	-290.4	-402
2001/10/31	-290.2	-270
1992/5/6	-287.6	-363
1990/4/8	-281.6	-262

Table 3
The 10 largest positive deviations (SI) Dst index and the corresponding value of Sym-H, 1985–2007.

yyyy/mm/dd	Dst (nT)	Sym-H (nT)
1991/3/24	129.0	145
1990/7/28	115.5	149
2001/3/29	108.8	124
1999/6/26	102.8	102
1991/6/12	86.6	149
1989/1/20	86.2	85
2002/5/17	84.4	108
2004/10/31	81.0	95
1999/7/25	79.6	75
2002/3/11	79.4	81

5. Summary

both indices are shown. The Sym-H spectrum has obvious peaks at one-day, half-day, and third-day, suggesting an incomplete removal of the Sq signal from the Sym-H index. In contrast, $Dst^{ASH-8507}$ shows no apparent peaks at these frequencies.

The USGS 1-min resolution Dst provides a technological advance in method and an improvement in time resolution while remaining consistent with the intent of the original Kyoto Dst index as a low-latitude disturbance signal. The increased time resolution allows for analysis of shorter time scale global features

such as sudden impulses and can provide an alternative to the use of Sym-H when a 1-min time resolution index is required for scientific analysis. On comparison to Sym-H, which is calculated from mid-latitude stations, strong differences are apparent during storm time.

Acknowledgments

We thank the Japan Meteorological Agency and the South African National Research Foundation for their commitment to the long-term operation, respectively, of the Kakioka and Hermanus magnetic observatories. We acknowledge Intermagnet (www.intermagnet.org) for its role in promoting high standards of magnetic-observatory practice. We thank the former World Data Center at Copenhagen, and the present World Data Centers at Kyoto and Edinburgh. We thank J.C. Green, C.A. Finn and T. White for reviewing a draft manuscript. We thank two anonymous referees for their reviews of the submitted draft manuscript. We thank E.A. McWhirter Jr. for help with data format conversion. This work and the present operation of the Honolulu and San Juan observatories are supported by the USGS Geomagnetism Program.

References

- Araki, T., Fujitani, S., Emoto, M., Yumoto, K., Shiodawa, K., Ichinose, T., Luehr, H., Orr, D., Milling, D.K., Singer, H., Rostoker, G., Tsunomura, S., Yamada, Y., Liu, C.F., 1997. Anomalous sudden commencement on March 24, 1991. *J. Geophys. Res.* 102 (A7), 14075–14086.
- Campbell, W.H., 1989. The regular geomagnetic field variations during quiet solar conditions. In: Jacobs, J.A. (Ed.), *Geomagnetism*, vol. 3. Academic Press, London, UK, pp. 385–460.
- Chapman, S., 1919. An outline of the theory of magnetic storms. *Proc. R. Soc. London Ser. A* 95, 61.
- Cl'ua de Gonzalez, A.L., Gonzalez, W.D., Dutra, S.L.G., Tsurutani, B.T., 1993. Periodic variation in the geomagnetic activity: a study based on the Ap index. *J. Geophys. Res.* 98, 9215–9231.
- Gonzalez, W.D., Joselyn, J.A., Kamide, Y., Kroehl, H.W., Rostoker, G., Tsurutani, B.T., Vasyliunas, V.M., 1994. What is a geomagnetic storm? *J. Geophys. Res.* 99, 5771.
- Iyemori, T., 1990. Storm-time magnetospheric currents inferred from mid-latitude geomagnetic field variations. *J. Geomagn. Geoelectr.* 42, 1249.
- Jackson, A., Finlay, C.C., 2007. Geomagnetic secular variation and its applications to the core. In: Kono, M. (Ed.), *Geomagnetism, Treatise on Geophysics*, vol. 5. Elsevier Science, New York, NY, pp. 147–193.
- Karinen, A., Mursula, K., 2006. A new reconstruction of the D_{st} index for 1932–2002. *J. Geophys. Res.* 11, A08207, doi:10.1029/2005JA011299.
- Love, J.J., 2008. Magnetic monitoring of Earth and space. *Phys. Today* 61, 31–37.
- Love, J.J., Gannon, J.L., 2009. Revised Dst and the epicyles of magnetic disturbance: 1958–2007. *Ann. Geophys.* 27, 3101–3131.
- McPherron, R.L., 1995. Magnetospheric dynamics. In: Russell, C.T., Kivelson, M.G. (Eds.), *Introduction to Space Physics*. Cambridge University Press, Cambridge, UK, pp. 400–458.
- Mendes, O., Mendes da Costa, A., Bertoni, F.C.P., 2006. Effects of the number of stations and time resolution on Dst derivation. *J. Atmos. Solar Terr. Phys.* 68, 2127–2137.
- Press, W.H., Teukolsky, S.A., Vetterling, W.T., Flannery, B.P., 2007. *Numerical Recipes 3rd Edition: The Art of Scientific Computing*. Cambridge University Press, Cambridge.
- Purucker, M.E., Whaler, K.A., 2007. Crustal magnetism. In: Kono, M. (Ed.), *Geomagnetism, Treatise on Geophysics*, vol. 5. Elsevier Science, New York, NY, pp. 195–235.
- Reeves, G.D., McAdams, K.L., Friedel, R.H.W., O'Brien, T.P., 2003. Acceleration and loss of relativistic electrons during geomagnetic storms. *Geophys. Res. Lett.* 30 (10), 1529, doi:10.1029/2002GL016513.
- Russell, C.T., 2000. The solar wind interaction with the Earth's magnetosphere: a tutorial. *IEEE Trans. Plasma Sci.* 28, 1818–1830.
- Sugiura, M., 1964. Hourly values of equatorial Dst for the IGY. *Ann. Int. Geophys. Year* 35, 9–45.
- Sugiura, M., Hendricks, S., 1967. Provisional hourly values of equatorial Dst for 1961, 1962, and 1963. Technical Note D-4047, NASA, Washington, DC.
- Sugiura, M., Kamei, T., 1991. Equatorial Dst index 1957–1986. IAGA Bull., 40, ISGI Pub. Ofce, Saint-Maur-des-Fosses, France.
- Wanliss, J.A., Showalter, K.M., 2006. High-resolution global storm index: Dst versus SYM-H. *J. Geophys. Res.* 111, A02202, doi:10.1029/2005JA011034.